Journal of Materials Chemistry A

ROYAL SOCIETY OF CHEMISTRY

COMMUNICATION

View Article Online
View Journal | View Issue

Check for updates

Cite this: *J. Mater. Chem. A*, 2025, **13**, 28887

Received 6th April 2025
Accepted 13th August 2025

DOI: 10.1039/d5ta02720a

rsc.li/materials-a

Thermally polymerizable phthalocyanine realizes a metal–nitrogen-doped carbon material featuring a defined single-atom catalyst motif with CO_2RR activity

Yuki Sano,[a] Daichi Nakajima,[a] Biplab Manna,[b] Koki Chida,[c] Ryojun Toyoda,*[a] Shinya Takaishi,[a] Kazuyuki Iwase,*[c] Koji Harano,[bd] Yuta Nishina,[ef] Takeharu Yoshii[c] and Ryota Sakamoto*[ag]

Metal–nitrogen-doped carbon materials (MNCs) exhibit good electrocatalytic performance owing to the intrinsic advantages of carbon-based materials and the presence of isolated and stabilized metal atoms coordinated by nitrogen sites. However, conventional high-temperature pyrolysis of precursor molecules make it difficult to control the coordination structure precisely. To address this issue, here we report a new synthesis strategy for MNCs. Specifically, we design and synthesize Ni-phthalocyanine functionalized with ethynyl groups as solid-state thermal polymerization points. After depositing the Ni-phthalocyanine precursor on a carbon support and performing a thermal treatment, the resultant carbon composite material features a Ni–N_4 coordination structure derived from the precursor, and enhanced porosity. This material demonstrates high catalytic activity for the CO_2 reduction reaction (CO_2RR). Our synthetic approach is applicable to various precursor molecules and carbon supports, paving the way for the further development of MNC-based electrode catalysts.

Introduction

In recent years, extensive research and development efforts have been devoted to various energy conversion technologies, such as water electrolysis,[1–3] fuel cells,[4,5] metal–air batteries,[6,7] CO_2 reduction reactions,[8,9] and N_2 reduction reactions,[10,11] to address the pressing issues of the energy crisis and global warming. Noble metal-based catalysts, including Pt, Au, and Ag, are known to function as electrocatalysts in these technologies, demonstrating exceptional performance.[12–17] However, their high cost and limited availability impose significant constraints on large-scale commercialization.[18] Consequently, there is a growing demand for the development of alternative catalyst materials that can serve as viable substitutes.[19]

Single-atom catalyst (SAC), in which metal atoms are dispersed in an isolated atomic state, has earned significant attention as a novel catalyst material.[20] Due to its inherent electronic structure, SAC exhibits high catalytic activity and selectivity. Moreover, maximizing atomic utilization efficiency enables a substantial reduction in the consumption of catalytic metals, making it a promising candidate for sustainable catalyst development.[21]

SAC requires a support substrate to immobilize metal atoms, and various materials, including metal oxides[22,23] and metal–organic frameworks[24,25] (MOFs), have been investigated. Among them, metal–nitrogen-doped carbon materials (MNCs), which feature metal atoms coordinated to doped nitrogen sites, exhibit excellent performance as SAC due to its isolated and stabilized metal atoms at nitrogen sites, as well as its superior properties derived from carbon materials such as mechanical properties, specific surface area, electronic conductivity, structural flexibility, low cost, and chemical stability.[26–29]

MNCs have been applied in various catalytic reactions such as oxygen reduction reaction[27–29] (ORR), hydrogen evolution reaction[30,31] (HER), oxygen evolution reaction[32] (OER), and carbon dioxide reduction reaction[33,34] (CO_2RR). In particular, CO_2RR, which electrochemically reduces CO_2 to produce more valuable compounds, is regarded as one of the essential technologies for achieving carbon neutrality and has been researched actively.[35] For example, Su *et al.* reported the synthesis of an MNC with Ni–N coordination sites through thermal treatment of an organometallic complex containing Ni–N bonds and its application as a CO_2RR electrocatalyst,

[a]*Department of Chemistry, Graduate School of Science, Tohoku University, 6-3 Aramaki Aza-Aoba, Aoba-ku, Sendai 980-8578, Japan. E-mail: ryojun.toyoda.a8@tohoku.ac.jp; ryota.sakamoto.e3@tohoku.ac.jp*

[b]*Center for Basic Research on Materials, National Institute for Materials Science, 1-1 Namiki, Tsukuba, Ibaraki 305-0044, Japan*

[c]*Institute of Multidisciplinary Research for Advanced Materials, Tohoku University, 2-1-1 Katahira, Aoba-ku, Sendai, Miyagi, 980-8577, Japan. E-mail: kazuyuki.iwase.a6@tohoku.ac.jp*

[d]*Research Center for Autonomous Systems Materialogy (ASMat), Institute of Integrated Research, Institute of Science Tokyo, 4259 Nagatsuda-cho, Midori-ku, Yokohama, Kanagawa 226-8501, Japan*

[e]*Graduate School of Natural Science and Technology, Okayama University, 3-1-1 Tsushimanaka, Kita-ku, Okayama 700-8530, Japan*

[f]*Research Institute for Interdisciplinary Science, Okayama University, 3-1-1 Tsushimanaka, Kita-ku, Okayama 700-8530, Japan*

[g]*Division for the Establishment of Frontier Sciences of Organization for Advanced Studies at Tohoku University, 2-1-1 Katahira, Aoba-ku, Sendai 980-8577, Japan*

demonstrating Faraday efficiency for CO production (FE_{CO}) exceeding 90%.[36] Similarly, Pan *et al.* demonstrated that an MNC with atomically dispersed Co–N_5 sites achieved FE_{CO} above 90% and sustained both current density and FE_{CO} for 10 hours of continuous operation.[37] These findings highlight the high reaction selectivity and excellent stability of MNCs, and numerous reports of MNCs with outstanding CO_2RR electrocatalytic performance have since followed.[38–47]

MNCs intended for SAC applications are typically synthesized through high-temperature pyrolysis of selected precursors under a controlled atmosphere, such as inert gases (N_2, Ar) or nitrogen sources[48] (*e.g.* NH_3). Mixtures of carbon matrix, nitrogen precursors, and metal sources,[49,50] or MOFs[51,52] are typically used as precursors, and it is considered that by modifying the composition and structure of precursors, the binding energy and the form of bonding between the catalyst and reactant molecules can be efficiently adjusted, thereby modulating catalytic activity.[53,54] However, in practice, due to complex pyrolysis reactions during thermal treatment, active sites formed by metal centers coordinated to nitrogen atoms possess diverse coordination structures, making it difficult to precisely control their structure.[55] As a result, the coordination structures of MNCs remain unclear, which means it is difficult to conduct detailed studies of reaction mechanisms using DFT calculations.[55] Furthermore, the electronic properties of the metal atoms and their corresponding catalytic reactions are greatly influenced by the coordination environment, which makes controlling catalytic reactions challenging due to the complicated coordination structures.[56] Therefore, to address these challenges and further enhance the practicality of MNCs, the development of new synthetic methods that can achieve both precisely controlled coordination structures and superior performance is necessary.

In this study, we propose a novel strategy for synthesizing MNCs by embedding well-defined chemical structures into carbon frameworks using precursor molecules bearing thermally polymerizable groups. In this approach, the nanocrystallized precursor molecules are first supported on carbon materials, which play a crucial role in their uniform distribution and stabilization as active centers.[57,58] Subsequent thermal treatment facilitates the formation of a composite in which the precursor structure is embedded within the carbon matrix. Furthermore, the introduction of thermally polymerizable groups enables polymerization and carbonization to occur at temperatures lower than the decomposition point of the precursors, thereby allowing the chemical structure of the precursor to be precisely retained.[59] Specifically, we design and synthesize a nickel phthalocyanine molecule (**Ni-OEPPc**) with eight ethynyl groups as thermally polymerizable functional groups, which is supported on a carbon substrate, and then thermally polymerized and carbonized (Fig. 1). The combination of this synthesis method using thermal polymerization and carbon supporting of precursors is expected to enable the synthesis of carbon materials that simultaneously achieve the desired chemical structure and pore structure and maximize the potential of the introduced chemical structure. In this paper, we also demonstrate that the resultant MNC has SAC centers and evaluate its CO_2RR ability.

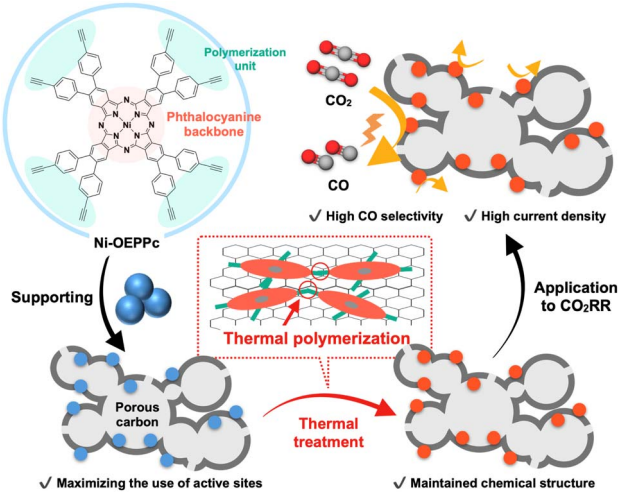

Fig. 1 Strategy of this study for the creation of metal–nitrogen-doped carbon materials.

Results and discussion

To demonstrate the strategy for MNCs creation, we designed and synthesized a new compound, [2,3,9,10,16,17,23,24-octakis(4-ethynylphenyl)phthalocyaninato]nickel(II) (**Ni-OEPPc**, Fig. 1), which is a nickel phthalocyanine derivative with thermal polymerization groups, as the precursor and aimed to introduce the Ni–N_4 coordination structure into carbon materials (Fig. 1). Phthalocyanines possess high thermal and chemical stability, as well as robust redox activity.[60] Due to these characteristics, their metal centers are known to exhibit high performance as active sites for various electrocatalytic reactions.[61–68] Specifically, unsubstituted nickel phthalocyanine (**Ni-Pc**) has been reported to show high CO selectivity (FE > 90%) as an active site for CO_2RR.[69–73] However, a molecular material generally has low electrical conductivity, and its durability at high current density is a concern.[74–76] Therefore, in this study, we attempted to synthesize carbon materials that precisely maintain the Ni–N_4 coordination structure, analyzed their structure, and then investigated the CO_2RR electrocatalytic performance of the resulting materials. The synthesis of **Ni-OEPPc** was carried out according to the synthetic route shown in Fig. S1. The successful synthesis of compounds **2**, **3**, and **4** was confirmed by NMR and mass spectrometry (Fig. S2–S11). **Ni-OEPPc** was obtained from **4** as a solid product *via in situ* deprotection and precipitation.[77] An excess amount of tetrabutylammonium fluoride was added dropwise to a solution of **4** in anhydrous tetrahydrofuran under a nitrogen atmosphere. The obtained green solid precipitate of **Ni-OEPPc** was isolated by filtration. The success of the synthesis was confirmed by infrared spectroscopy and mass spectrometry (Fig. S12 and S13). Hereafter, a **Ni-OEPPc** sample subjected to thermal treatment is referred to as **Ni-OEPPc_*x*** (*x* denotes the calcination temperature), while that on a carbon support (CNovel 010-00®)[78] is referred to as **Ni-**

OEPPc/C. A **Ni-OEPPc** sample which was calcined after being supported on the carbon support is expressed as **Ni-OEPPc/C_*x***.

To gain a deeper understanding of the structure of **Ni-OEPPc** after thermal treatment, **Ni-OEPPc** was subjected to thermal treatment alone, and its structure after thermal treatment was analyzed. Thermal treatments of **Ni-OEPPc** were carried out under an Ar atmosphere at different calcination temperatures at a heating rate of 10 °C min^{-1}. The thermal behavior of **Ni-OEPPc** was investigated by thermogravimetry-differential thermal analysis (TG-DTA) and compared with unsubstituted **Ni-Pc**. Fig. 2 shows the weight changes measured by TG and the DTA curves for **Ni-OEPPc** and **Ni-Pc**. DTA measurements revealed an exothermic peak observed only for **Ni-OEPPc** around 215 °C, which is considered to be associated with thermal polymerization.[79] The progress of the polymerization reaction of the ethynyl groups was also confirmed by other measurements. In IR spectra, two peaks attributed to the vibrations of the ethynyl group were observed before thermal treatment at 3273 cm^{-1} (C–H) and 2099 cm^{-1} (C≡C).[80] However, these absorption peaks disappeared after thermal treatment at 250 °C (**Ni-OEPPc_250**), suggesting that the ethynyl groups were converted during thermal treatment (Fig. S14). Furthermore, in solid-state ^{13}C NMR measurements of **Ni-OEPPc** and **Ni-OEPPc_250**, the spectra before thermal treatment exhibited multiple peaks in the 100–150 ppm range derived from aromatic carbon, along with peaks around 70–80 ppm attributed to sp bonding. In contrast, after thermal treatment, a reduction in the sp bonding and broadening of the aromatic carbon-derived peaks were observed, indicating that the polymerization reaction proceeded during thermal treatment (Fig. S15). TG measurements revealed that **Ni-OEPPc** exhibited only a 6% weight loss at 700 °C, demonstrating excellent thermal stability. To investigate the thermal stability durability of polymerized **Ni-OEPPc** at higher temperatures above 700 °C, TG-DSC for **Ni-OEPPc** was conducted up to 1600 °C (Fig. S16), disclosing that 80% of the initial weight was retained with the formation of a graphitic structure (Fig. S17). In contrast, **Ni-Pc** showed a 37% weight loss at the same temperature. From these results, it is considered that thermal polymerization of the ethynyl groups and subsequent carbonization suppresses decomposition of the phthalocyanine macrocycle. Additionally, thermogravimetry–differential scanning calorimetry–mass spectroscopy (TG-DSC-MS) was used to analyze the volatile components during thermal treatment. The detected chemical species were derived from partial structures other than the phthalocyanine ring (Fig. S18).

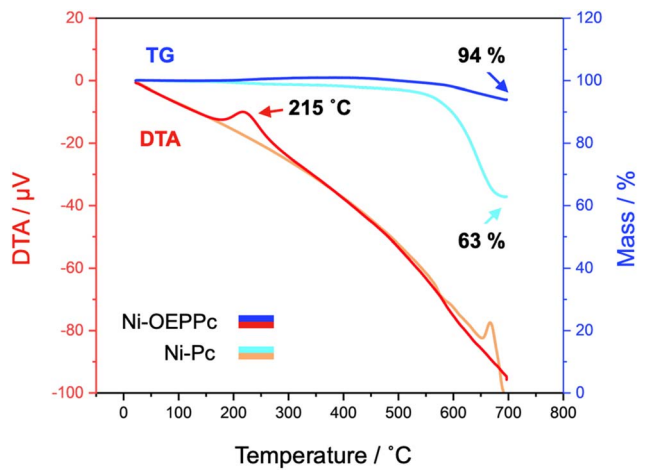

Fig. 2 TG-DTA curves of Ni-OEPPc and Ni-Pc. Dark and light colors correspond to those of Ni-OEPPc and Ni-Pc, respectively.

Ni-OEPPc after thermal treatment was structurally characterized by Raman spectroscopy, infrared (IR) spectroscopy, electrical conductivity test, X-ray photoelectron spectroscopy (XPS), X-ray absorption fine structure (XAFS) analysis, X-ray diffraction (XRD), and nitrogen adsorption measurement. Raman spectroscopy was performed at different thermal treatment temperatures, and up to 700 °C, a series of Raman peaks derived from the phthalocyanine macrocycle were observed at approximately 650 cm^{-1}–750 cm^{-1} and 1100 cm^{-1}–1600 cm^{-1}, suggesting that the coordination structure was retained at this temperature (Fig. S19). In contrast, the metal phthalocyanine-derived peaks disappeared in **Ni-OEPPc_800**, and broad peaks were observed at 1336 cm^{-1} and 1592 cm^{-1} (Fig. S19), corresponding to the D and G bands, respectively. Given the high I_D/I_G ratio, these features indicate the formation of a defect-rich carbonaceous framework.[81,82] Similarly, The IR spectra confirmed that absorption peaks in the fingerprint region were maintained after thermal treatment up to 700 °C (Fig. S20). Electrical conductivity measurements revealed that **Ni-OEPPc** was initially insulating (2×10^{-8} S m^{-1}), but its conductivity significantly increased with higher thermal treatment temperatures. Notably, **Ni-OEPPc_700** exhibited excellent electrical conductivity of 1.2×10^{-1} S m^{-1}, indicating the progression of carbonization as the temperature increased (Table S1). This enhanced electrical conductivity is likely governed by multiple mechanisms, including hopping conduction and tunneling conduction between sp^2 domains, as well as charge transport through partially graphitized sp^2 carbon structures, all of which are intricately involved.[83,84] XPS measurements and analysis of the N 1s and Ni 2p spectra showed that the overall spectral features of **Ni-OEPPc** were consistent with previously reported XPS spectra of Ni-Pc.[85] The Ni $2p_{3/2}$ spectrum of **Ni-OEPPc_700** exhibited slight broadening, which may be attributed to the presence of a small amount of oxidized Ni species, carbides, or metallic Ni.[86] In addition, the N 1s spectrum of **Ni-OEPPc_700** revealed additional components attributed to graphitic N and pyrrolic N, which are likely due to the thermal transformation of certain nitrogen-containing structures within **Ni-OEPPc** during the carbonization process (Fig. S21). In the X-ray absorption near edge structure (XANES) spectrum of **Ni-OEPPc** (Fig. 3a), a shoulder peak was observed around 8335 eV (1s → $4p_z$ transition), which is characteristic of square-planar configuration with high metal–N_4 (M–N_4) symmetry.[87] Additionally, in the white line region, peaks derived from the convolution of the 1s → $4p_{x,y}$ transitions and multiple scattering processes were observed.[87] In previous studies, it has been reported that MNCs derived from **Ni-Pc** exhibit XANES spectra different from those of **Ni-Pc**,[88,89] and this difference has been attributed to the loss

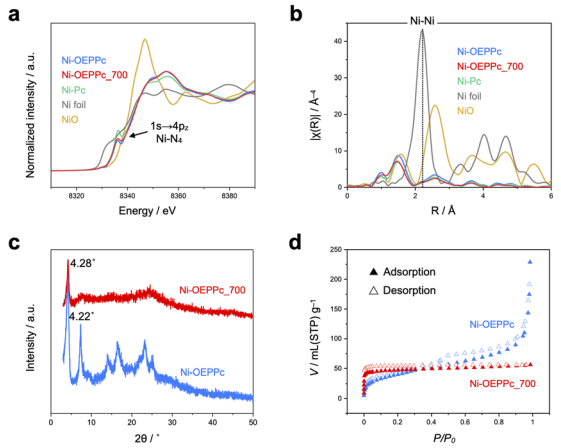

Fig. 3 (a) XANES spectra of **Ni-OEPPc** and **Ni-OEPPc_700**. (b) EXAFS spectra of **Ni-OEPPc** and **Ni-OEPPc_700**, together with those of **Ni-Pc**, Ni foil, and NiO as references. (c) XRD patterns of **Ni-OEPPc** and **Ni-OEPPc_700**. (d) Nitrogen adsorption and desorption isotherms at 77 K for **Ni-OEPPc** and **Ni-OEPPc_700**.

of Ni–N fragments around Ni atoms during thermal treatment, leaving the unsaturated M–N_x moieties.[90] Meanwhile, **Ni-OEPPc_700** exhibited a similar XANES spectrum, which means the Ni–N_4 coordination structure was strictly preserved after thermal treatment. Moreover, the EXAFS spectra of both **Ni-OEPPc** and **Ni-OEPPc_700** were nearly identical, and no Ni–Ni peak (2.18 Å) was detected[91] (Fig. 3b). This suggests that metal aggregation did not occur during thermal treatment, which is consistent with the XPS measurement and the XRD measurement results discussed later. Furthermore, the EXAFS spectrum of **Ni-OEPPc_700** was fitted (Fig. S22b and Table S2). As a result, the experimental spectra are reproduced with a tetra-coordination structure, indicating that the Ni–N_4 coordination structure of mother **Ni-OEPPc** is maintained. XRD measurements were conducted to analyze the structural periodicity of **Ni-OEPPc** before and after thermal treatment (Fig. 3c). Before heating, multiple peaks originating from the crystalline structure of **Ni-OEPPc** were observed, with the sharpest peak appearing at 4.12° (20.93 Å). This peak was also present in **Ni-OEPPc_700**, which implies that the precursor-derived ordered structure was partially retained even after thermal treatment at 700 °C.[92,93] The porosity and pore structure were evaluated through nitrogen adsorption measurements at 77 K (Fig. 3d). The adsorption–desorption isotherm of **Ni-OEPPc** exhibited a rapid gas uptake up to a low relative pressure (P/P_0), confirming the presence of micropores. The specific surface area of **Ni-OEPPc**, determined by Brunauer–Emmett–Teller (BET) method, was 144 $m^2\ g^{-1}$. After thermal treatment, the shape of the isotherm changed, and **Ni-OEPPc_700** displayed a Type I isotherm. BET specific surface area of **Ni-OEPPc_700** increased to 184 $m^2\ g^{-1}$, indicating enhanced porosity. Pore size analysis using nonlocal density functional theory (NLDFT) further revealed the distribution of a large number of pores smaller than 1 nm (Fig. S23).

Next, introduction of the Ni–N_4 structure into the carbon material was carried out through the loading of **Ni-OEPPc** onto the carbon support and subsequent thermal treatment. The dispersibility of insoluble **Ni-OEPPc** was investigated using dynamic light scattering (DLS), which indicated that the particle size of **Ni-OEPPc** dispersed in tetrahydrofuran (THF) was approximately 20 nm to 40 nm (Fig. S24b). Additionally, TEM images of **Ni-OEPPc** indicated good agreement with the result of DLS measurements (Fig. S25). Based on the above findings and the XRD results, **Ni-OEPPc** is considered to exist as highly crystalline particles on the nanoscale in THF. The loading of **Ni-OEPPc** onto the carbon support was carried out using the impregnation method. Dehydrated THF was added to **Ni-OEPPc** and the carbon support, and the mixture was subjected to ultrasonic treatment. The solvent was then removed, yielding the supported **Ni-OEPPc** sample, **Ni-OEPPc/C**. The morphology of **Ni-OEPPc/C** was observed using scanning transmission electron microscopy (STEM). The corresponding elemental maps obtained from energy-dispersive X-ray (EDX) analysis confirmed that N atoms and Ni atoms were uniformly dispersed on carbon, suggesting that **Ni-OEPPc** is uniformly supported on the carbon support (Fig. S26). In addition, a comparison of the XPS spectra of **Ni-OEPPc** and **Ni-OEPPc/C** revealed no significant differences in the position or shape of the Ni $2p_{3/2}$ peaks, suggesting that the oxidation state of Ni remained unchanged upon supporting. In the N 1s spectra, components corresponding to graphitic N and pyrrolic N were observed, which are considered to originate from nitrogen species inherently present in the carbon support (Fig. S27). Then, thermal treatment of **Ni-OEPPc/C** was performed. Considering the results of the thermal treatment of **Ni-OEPPc** alone, the temperature was raised to 700 °C, which was deemed appropriate for both maintaining the Ni–N_4 coordination structure and promoting carbonization. The process was conducted under an Ar atmosphere at a heating rate of 10 °C min^{-1}, yielding the supported and thermal-treated sample, **Ni-OEPPc/C_700**. The metal content of **Ni-OEPPc/C_700** was analyzed using inductively coupled plasma (ICP) analysis, revealing that the Ni wt% was approximately 1.2%, almost equal to the loading (1.07 wt%).

The structure of **Ni-OEPPc/C_700** after thermal treatment was investigated by XPS, XAFS, XRD, STEM, and nitrogen adsorption tests. XPS measurements of **Ni-OEPPc/C** and **Ni-OEPPc/C_700** showed similar spectral changes to those observed in thermally treated **Ni-OEPPc** alone (**Ni-OEPPc_700**). Specifically, a slight broadening of the Ni $2p_{3/2}$ peak and an increase in the components corresponding to graphitic N and pyrrolic N in the N1s spectrum were observed (Fig. S24). In XAFS measurements, an unsubstituted **Ni-Pc**-used composite (**Ni-Pc/C_700**) was synthesized for comparison (Fig. 4a and S28). The XANES spectra of **Ni-OEPPc/C** and **Ni-OEPPc/C_700** closely resembled that of **Ni-OEPPc**, implying that the Ni–N_4 coordination structure remained intact (Fig. 4a and S29). In contrast, a significant change in the shape of spectra was observed for **Ni-Pc/C_700**, indicating that the Ni–N_4 coordination structure was altered due to thermal decomposition (Fig. 4a). The EXAFS spectra of **Ni-OEPPc/C** and **Ni-OEPPc/C_700** were nearly identical, and no Ni–Ni peak (2.18 Å) was detected,[91] suggesting that metal aggregation did not occur during thermal treatment (Fig. S30). Ni–N_4 coordination structure of **Ni-OEPPc** is

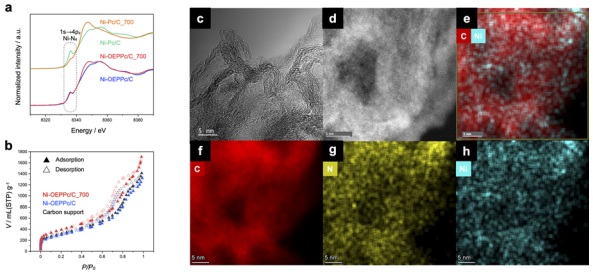

Fig. 4 (a) XANES spectra of **Ni-OEPPc/C**, **Ni-OEPPc/C_700**, **Ni-Pc/C**, and **Ni-Pc/C_700**. (b) Nitrogen adsorption and desorption isotherms at 77 K for **Ni-OEPPc/C**, **Ni-OEPPc/C_700**, and the carbon support. (c) Representative TEM image of **Ni-OEPPc/C_700**. (d–h) HAADF-STEM image of **Ni-OEPPc/C_700** and corresponding EDX maps of C/Ni overlay, C, N, and Ni, respectively.

maintained when **Ni-OEPPc** was heat-treated after it was loaded on carbon support (Fig. S22c and Table S2). The porosity of **Ni-OEPPc/C** and **Ni-OEPPc/C_700** was investigated using nitrogen adsorption measurements at 77 K. The results revealed that both **Ni-OEPPc/C** and **Ni-OEPPc/C_700** exhibited adsorption–desorption isotherms and pore size distributions using NLDFT similar to those of the carbon support (Fig. 4b and S31). This indicates that the pore structure derived from the carbon support was preserved. Fig. 4c and S32 show the representative TEM images of **Ni-OEPPc/C_700**, and Fig. 4d–h presents the HAADF-STEM image and the corresponding elemental maps obtained by EDX analysis. The elemental maps indicate that N and Ni atoms are uniformly distributed on carbon. Considering the results of the XAFS measurements, this suggests that in **Ni-OEPPc/C_700**, the Ni–N_4 structure is dispersed on carbon.

To investigate the CO_2RR activity of **Ni-OEPPc/C_700**, cyclic voltammetry (CV) measurements were conducted using a CO_2-saturated $KHCO_3$ solution and an Ar-saturated phosphate buffer solution. The increase in current under CO_2 conditions confirmed that **Ni-OEPPc/C_700** functions as a CO_2RR catalyst (Fig. S33). To further analyze the CO_2 reduction products generated by **Ni-OEPPc/C_700**, electrolysis was performed under static conditions for 30 min using a gas diffusion electrode (GDE) loaded with **Ni-OEPPc/C_700**. The gaseous CO_2 reduction products were then quantitatively analysed by gas chromatography. The dependence of FE_{H2} and FE_{CO} on current density is presented in Fig. 5a. At 10 mA cm^{-2}, **Ni-OEPPc/C_700** exhibited FE_{CO} of 84% at −0.56 V *vs.* reversible hydrogen electrode (RHE), demonstrating high activity for CO production. The reaction mechanism for CO_2 reduction is considered to be similar to that reported for SACs with M–N_4 coordination structures in previous studies[21,94–96] (Fig. S34). Furthermore, it maintained a FE_{CO} value of above 90% up to a current density of 150 mA cm^{-2} with TOF of 2.6 s^{-1} (9360 h^{-1}), which is relatively high or comparable to those of reported Ni-SACs (Tables S4–S6). A comparison of catalytic performance at 150 mA cm^{-2} among **Ni-OEPPc/C_700**, **Ni-Pc/C_700**, and **Ni-OEPPc/C** demonstrated that **Ni-OEPPc/C_700** exhibited the lowest overpotential and the highest FE_{CO}. These results indicate that both carbonization and the stabilization of the coordination structure enabled by the introduction of the ethynyl groups contribute to the enhancement of the catalytic performance (Fig. S35). In addition, measurements of the electrochemical surface area (ECSA) revealed a decrease in ECSA for **Ni-OEPPc/C_700** compared to **Ni-OEPPc/C**. Nevertheless, **Ni-OEPPc/C_700** exhibited higher specific activity at both 10 mA cm^{-2} and 150 mA cm^{-2}. These results further support that the enhanced performance of **Ni-OEPPc/C_700** is not attributed to an increase in ECSA, but rather to other factors, such as carbonization and the stabilization of the Ni–N_4 coordination structure induced by thermal treatment (Fig. S36 and Table S7). Furthermore, the FE_{CO} of **Ni-OEPPc_700** and **Ni-OEPPc_700/C** (**Ni-OEPPc** was calcined at 700 °C, and then deposited on the carbon substrate) were merely 10% and 23% at 10 mA cm^{-2} (Table S8), underscoring the importance of the deposition of **Ni-OEPPc_700** on the carbon support before calcination for enhancing the accessibility of the active metal sites. To quantify liquid products other than the main products (CO and H_2), the electrolyte after the reaction was analyzed using NMR spectroscopy. The results

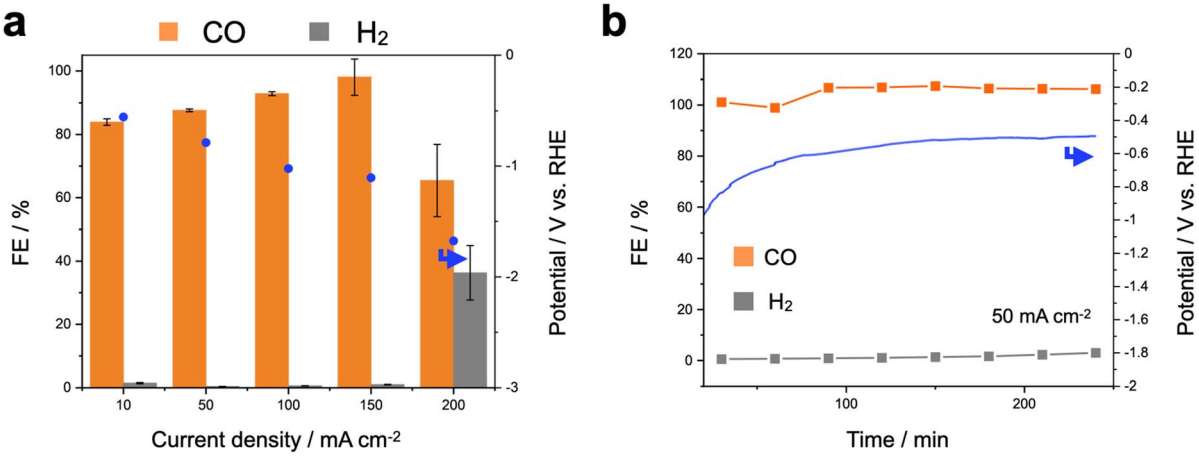

Fig. 5 (a) FE_{CO} and FE_{H2} for **Ni-OEPPc/C_700** at current densities of 10, 50, 100, 150, and 200 mA cm^{-2}. (b) Long-term test curves and FE of **Ni-OEPPc/C_700** for 4 h at 50 mA cm^{-2}.

revealed the presence of a very small amount of formic acid (approx. 0.1% at 10–150 mA cm^{-2}) (Table S9). Finally, the durability of **Ni-OEPPc/C_700** was analyzed under a constant current of 50 mA cm^{-2} (Fig. 5b and Table S10). Gas products were characterized every 30 min by gas chromatography, and the change in FE_{CO} was negligible for 4 h. In addition, XAFS measurements for **Ni-OEPPc/C_700** suggested that the valence and coordination structure of the nickel center remained unchanged before and after the CO_2 electrolysis (Fig. S37). Furthermore, the morphology of **Ni-OEPPc/C_700** was preserved before and after the CO_2RR operation (Fig. S38 and S39). These findings demonstrate that **Ni-OEPPc/C_700** retains its coordination structure under high current densities and prolonged electrolysis, thereby enabling sustained and efficient CO_2-to-CO conversion. To further evaluate the durability, long-term electrolysis was performed using a GDE with enhanced hydrophobicity achieved through PTFE treatment, as reported in a previous study,[97] with the electrolyte replaced every 2.5 h. As a result, **Ni-OEPPc/C_700** exhibited stable CO production at 50 mA cm^{-2} even after 10 h of operation (Fig. S40 and S41).

Conclusion

In this study, we aimed to develop carbon materials with well-defined chemical structures by exploring a novel approach to modifying the structure of carbon materials using molecules with thermally polymerizable groups and attempted to introduce the metal phthalocyanine structure into carbon materials. First, an analysis of the thermal properties of **Ni-OEPPc** revealed that polymerization proceeded at approximately 210–215 °C, and the chemical structure was retained even after thermal treatment at 700 °C. The preservation of the coordination structure was attributed to the strong Ni–N_4 coordination environment and the thermal polymerization induced by the ethynyl groups. Subsequently, **Ni-OEPPc** was supported on the carbon support and subjected to thermal treatment at 700 °C to modify the carbon material. The resulting **Ni-OEPPc/C_700** successfully maintained both the Ni–N_4 coordination structure and the pore structure derived from the carbon support. Results of XAFS analysis and Electron microscopy observations suggested that the Ni–N_4 coordination structure was uniformly distributed on the carbon support, indicating the successful synthesis of an MNC with a well-defined chemical structure. Furthermore, **Ni-OEPPc/C_700** exhibited high performance as a CO_2RR electrode catalyst, demonstrating efficient CO production at a high current density of 150 mA cm^{-2}, highlighting its excellent potential as a SAC. Although introducing thermally polymerizable groups into precursor molecules is not always facile, this method can be applied to other precursor molecules as well, enabling the modification of carbon materials with diverse coordination structures by selecting appropriate precursors. Additionally, by choosing suitable support materials based on the desired properties, it becomes possible to synthesize carbon materials that simultaneously achieve specific chemical structures and pore morphologies. Thus, this study is expected to contribute to the further advancement of MNCs development.

Author contributions

Yuki Sano: conceptualization, data curation, investigation, formal analysis, writing original manuscripts, review, and editing. Daichi Nakajima: investigation. Biplab Manna: investigation, formal analysis. Koki Chida: investigation. Ryojun Toyoda: funding acquisition, methodology, resource, writing original manuscripts, review, and editing. Shinya Takaishi: methodology, resource. Kazuyuki Iwase: formal analysis, funding acquisition, investigation, methodology, resource, writing review, and editing. Koji Harano: formal analysis, funding acquisition, investigation, resource, writing review, and editing. Yuta Nishina: formal analysis, funding acquisition, investigation, resource, writing review, and editing. Takeharu Yoshii: investigation, funding acquisition. Ryota Sakamoto: conceptualization, formal analysis, funding acquisition, methodology, project administration, resource, supervision, writing original manuscripts, review, and editing.

Conflicts of interest

There are no conflicts to declare.

Data availability

The data supporting this article have been included as part of the SI.

Experimental details; Synthetic scheme of **Ni-OEPPc**; Characterization data for the small molecules; IR and solid-state ^{13}C NMR spectra for **Ni-OEPPc** and **Ni-OEPPc_250**; TG-DSC for **Ni-OEPPc** up to 1600 °C; XRD for **Ni-OEPPc**, **Ni-OEPPc_700**, **Ni-OEPPc_1600**; TG-DSC-MS for **Ni-OEPPc**; Raman and IR spectra, XPS of **Ni-OEPPc** before and after calcination; EXAFS fitting curves of Ni foil, **Ni-OEPPc_700**, **Ni-OEPPc/C_700**; Pore size distributions using NLDFT method for **Ni-OEPPc_700**; Photograph and particle size distribution for **Ni-OEPPc** suspension; Bright-field TEM image of **Ni-OEPPc**; HAADF-STEM image and EDX mapping for of **Ni-OEPPc/C**; XPS of **Ni-OEPPc**, **Ni-OEPPc/C**, and **Ni-OEPPc/C_700**; EXAFS for **Ni-OEPPc/C_700**, **Ni-OEPPc/C**, **Ni-Pc/C_700**, and **Ni-Pc/C**; XANES and EXAFS for **Ni-OEPPc**, **Ni-OEPPc/C**, **Ni-OEPPc/C_700**, **Ni-Pc**, Ni foil, and NiO; Pore size distributions for **Ni-OEPPc/C**, **Ni-OEPPc/C_700**, and the carbon support; TEM images of **Ni-OEPPc/C_700**; Cyclic voltammograms of **Ni-OEPPc/C_700** in CO_2 saturated 1 M $KHCO_3$; Proposed reaction pathway of CO_2 reduction to CO on Ni SAC; FE and potential between **Ni-OEPPc/C_700**, **Ni-OEPPc/C**, and **Ni-Pc/C_700**; Cyclic voltammograms of **Ni-OEPPc/C_700** and **Ni-OEPPc/C**; XANES and EXAFS spectra of **Ni-OEPPc/C_700** after electrolysis; SEM images of **Ni-OEPPc/C_700** after electrolysis; Further long-term measurement of **Ni-OEPPc/C_700**; Electrical conductivity; EXAFS fitting parameters; Actual measured values of electrolysis; Summary of reported Ni-SAC; Faraday efficiency for **Ni-OEPPc_700** and **Ni-OEPPc_700/C**; ECSA and specific activity of **Ni-OEPPc/C_700** and **Ni-OEPPc/C**; Faraday efficiency of formic acid for **Ni-OEPPc/C_700**. See DOI: **https://doi.org/10.1039/d5ta02720a**.

Acknowledgements

The present work was supported chiefly by JST-CREST (JPMJCR24S6 to Y. N., T. Y., and R. S.). This work was partially supported by JST-FOREST (JPMJFR203F to R. S.) and JST-PRESTO (JPMJPR2371 to K. I.; JPMJPR23QA to T. Y.; JPMJPR22Q5 to R. T.). JSPS KAKENHI (Grant No. JP25H01644, JP25H01999, JP24K01494, JP24H01690, JP23H04874) supports partly the present work. The Asahi Glass Foundation supports partly the resent work (to R. S.). The XAS measurement was conducted on the BL01B1 and BL14B2 beamlines at the SPring-8 facility (Proposal No. 2025A1811, 2024B1682, and 2023B2097). Y. S. acknowledges a financial support by GP-MS at Tohoku University.

Notes and references

1 M. Chatenet, B. G. Pollet, D. R. Dekel, F. Dionigi, J. Deseure, P. Millet, R. D. Braatz, M. Z. Bazant, M. Eikerling, I. Staffell, P. Balcombe, Y. Shao-Horn and H. Schäfer, *Chem. Soc. Rev.*, 2022, **51**, 4583–4762.
2 A. Raveendran, M. Chandran and R. Dhanusuraman, *RSC Adv.*, 2023, **13**, 3843–3876.
3 A. Rapakousiou, S. G. Chalkidis, M. P. Minadakis, M. L. Ruiz-González, C. Navio, G. C. Vougioukalakis and N. Tagmatarchis, *J. Mater. Chem. A*, 2025, **13**, 17489–17498.
4 O. Z. Sharaf and M. F. Orhan, *Renewable Sustainable Energy Rev.*, 2014, **32**, 810–853.
5 X. Zhao and K. Sasaki, *Acc. Chem. Res.*, 2022, **55**, 1226–1236.
6 L. Li, Z. Chang and X.-B. Zhang, *Adv. Sustainable Syst.*, 2017, **1**, 1700036.
7 X.-W. Lv, Z. Wang, Z. Lai, Y. Liu, T. Ma, J. Geng and Z.-Y. Yuan, *Small*, 2024, **20**, 2306396.
8 S. Zhang, Q. Fan, R. Xia and T. J. Meyer, *Acc. Chem. Res.*, 2020, **53**, 255–264.
9 Y. Lei, Z. Wang, A. Bao, X. Tang, X. Huang, H. Yi, S. Zhao, T. Sun, J. Wang and F. Gao, *Chem. Eng. J.*, 2023, **453**, 139663.
10 X. Cui, C. Tang and Q. Zhang, *Adv. Energy Mater.*, 2018, **8**, 1800369.
11 Z. Huang, M. Rafiq, A. R. Woldu, Q.-X. Tong, D. Astruc and L. Hu, *Coord. Chem. Rev.*, 2023, **478**, 214981.
12 C. Kim, H. S. Jeon, T. Eom, M. S. Jee, H. Kim, C. M. Friend, B. K. Min and Y. J. Hwang, *J. Am. Chem. Soc.*, 2015, **137**, 13844–13850.
13 W. Zhu, R. Michalsky, Ö. Metin, H. Lv, S. Guo, C. J. Wright, X. Sun, A. A. Peterson and S. Sun, *J. Am. Chem. Soc.*, 2013, **135**, 16833–16836.
14 W. Sheng, S. Kattel, S. Yao, B. Yan, Z. Liang, C. J. Hawxhurst, Q. Wu and J. G. Chen, *Energy Environ. Sci.*, 2017, **10**, 1180–1185.
15 Y. Zeng, J. Liang, C. Li, Z. Qiao, B. Li, S. Hwang, N. N. Kariuki, C.-W. Chang, M. Wang, M. Lyons, S. Lee, Z. Feng, G. Wang, J. Xie, D. A. Cullen, D. J. Myers and G. Wu, *J. Am. Chem. Soc.*, 2023, **145**, 17643–17655.
16 W. Xu, Z. Wang, P. Liu, X. Tang, S. Zhang, H. Chen, Q. Yang, X. Chen, Z. Tian, S. Dai, L. Chen and Z. Lu, *Adv. Mater.*, 2024, **36**, 2306062.
17 T. Yamada, K. Iwase, N. Todoroki and I. Honma, *ACS Appl. Energy Mater.*, 2025, **8**, 821–829.
18 A. Kumar, V. K. Vashistha, D. K. Das, S. Ibraheem, G. Yasin, R. Iqbal, T. A. Nguyen, R. K. Gupta and Md. Rasidul Islam, *Fuel*, 2021, **304**, 121420.
19 H. Cui, Y. Guo, L. Guo, L. Wang, Z. Zhou and Z. Peng, *J. Mater. Chem. A*, 2018, **6**, 18782–18793.
20 X.-F. Yang, A. Wang, B. Qiao, J. Li, J. Liu and T. Zhang, *Acc. Chem. Res.*, 2013, **46**, 1740–1748.
21 M. Li, H. Wang, W. Luo, P. C. Sherrell, J. Chen and J. Yang, *Adv. Mater.*, 2020, **32**, 2001848.
22 R. Lang, X. Du, Y. Huang, X. Jiang, Q. Zhang, Y. Guo, K. Liu, B. Qiao, A. Wang and T. Zhang, *Chem. Rev.*, 2020, **120**, 11986–12043.
23 M. J. Hülsey, S. Wang, B. Zhang, S. Ding and N. Yan, *Acc. Chem. Res.*, 2023, **56**, 561–572.
24 A. M. Abdel-Mageed, B. Rungtaweevoranit, M. Parlinska-Wojtan, X. Pei, O. M. Yaghi and R. J. Behm, *J. Am. Chem. Soc.*, 2019, **141**, 5201–5210.
25 S. Ma, W. Han, W. Han, F. Dong and Z. Tang, *J. Mater. Chem. A*, 2023, **11**, 3315–3363.
26 J. Guo, J. Huo, Y. Liu, W. Wu, Y. Wang, M. Wu, H. Liu and G. Wang, *Small Methods*, 2019, **3**, 1900159.
27 M. Fan, J. Cui, J. Wu, R. Vajtai, D. Sun and P. M. Ajayan, *Small*, 2020, **16**, 1906782.
28 J. Rong, E. Gao, N. Liu, W. Chen, X. Rong, Y. Zhang, X. Zheng, H. Ao, S. Xue, B. Huang, Z. Li, F. Qiu and Y. Qian, *Energy Storage Mater.*, 2023, **56**, 165–173.
29 H. Tian, A. Song, P. Zhang, K. Sun, J. Wang, B. Sun, Q. Fan, G. Shao, C. Chen, H. Liu, Y. Li and G. Wang, *Adv. Mater.*, 2023, **35**, 2210714.
30 W. Chen, J. Pei, C.-T. He, J. Wan, H. Ren, Y. Wang, J. Dong, K. Wu, W.-C. Cheong, J. Mao, X. Zheng, W. Yan, Z. Zhuang, C. Chen, Q. Peng, D. Wang and Y. Li, *Adv. Mater.*, 2018, **30**, 1800396.
31 S. Aralekallu, L. K. Sannegowda and V. Singh, *Int. J. Hydrogen Energy*, 2023, **48**, 16569–16592.
32 L. Cao, Q. Luo, J. Chen, L. Wang, Y. Lin, H. Wang, X. Liu, X. Shen, W. Zhang, W. Liu, Z. Qi, Z. Jiang, J. Yang and T. Yao, *Nat. Commun.*, 2019, **10**, 4849.
33 A. S. Varela, N. Ranjbar Sahraie, J. Steinberg, W. Ju, H.-S. Oh and P. Strasser, *Angew. Chem., Int. Ed.*, 2015, **54**, 10758–10762.
34 K. Iwase, K. Ebner, J. S. Diercks, V. A. Saveleva, S. Ünsal, F. Krumeich, T. Harada, I. Honma, S. Nakanishi, K. Kamiya, T. J. Schmidt and J. Herranz, *ACS Appl. Mater. Interfaces*, 2021, **13**, 15122–15131.
35 A. Fauzi, X. Chen, H. Zhao, S. Cao, L. Kong, S. Huang, S. Zhang and X. Ma, *Next Energy*, 2023, **1**, 100045.
36 P. Su, K. Iwase, S. Nakanishi, K. Hashimoto and K. Kamiya, *Small*, 2016, **12**, 6083–6089.
37 Y. Pan, R. Lin, Y. Chen, S. Liu, W. Zhu, X. Cao, W. Chen, K. Wu, W.-C. Cheong, Y. Wang, L. Zheng, J. Luo, Y. Lin, Y. Liu, C. Liu, J. Li, Q. Lu, X. Chen, D. Wang, Q. Peng, C. Chen and Y. Li, *J. Am. Chem. Soc.*, 2018, **140**, 4218–4221.
38 Y. Chen, J. Zhang, L. Yang, X. Wang, Q. Wu and Z. Hu, *Electrochem. Energy Rev.*, 2022, **5**, 11.

39 Z. Shi, W. Yang, Y. Gu, T. Liao and Z. Sun, *Adv. Sci.*, 2020, **7**, 2001069.
40 H.-Y. Jeong, M. Balamurugan, V. S. K. Choutipalli, E. Jeong, V. Subramanian, U. Sim and K. T. Nam, *J. Mater. Chem. A*, 2019, **7**, 10651–10661.
41 J. Gu, C.-S. Hsu, L. Bai, H. M. Chen and X. Hu, *Science*, 2019, **364**, 1091–1094.
42 L. Lin, H. Li, C. Yan, H. Li, R. Si, M. Li, J. Xiao, G. Wang and X. Bao, *Adv. Mater.*, 2019, **31**, 1903470.
43 C.-S. Hsu, J. Wang, Y.-C. Chu, J.-H. Chen, C.-Y. Chien, K.-H. Lin, L. D. Tsai, H.-C. Chen, Y.-F. Liao, N. Hiraoka, Y.-C. Cheng and H. M. Chen, *Nat. Commun.*, 2023, **14**, 5245.
44 J. Wang, Y.-C. Huang, Y. Wang, H. Deng, Y. Shi, D. Wei, M. Li, C.-L. Dong, H. Jin, S. S. Mao and S. Shen, *ACS Catal.*, 2023, **13**, 2374–2385.
45 S. Wang, A. Badreldin and Y. Li, *Chem. Commun.*, 2025, **61**, 10484–10504.
46 Z.-L. Wang, J. Choi, M. Xu, X. Hao, H. Zhang, Z. Jiang, M. Zuo, J. Kim, W. Zhou, X. Meng, Q. Yu, Z. Sun, S. Wei, J. Ye, G. G. Wallace, D. L. Officer and Y. Yamauchi, *ChemSusChem*, 2020, **13**, 929–937.
47 Y. Zhou, Q. Zhou, H. Liu, W. Xu, Z. Wang, S. Qiao, H. Ding, D. Chen, J. Zhu, Z. Qi, X. Wu, Q. He and L. Song, *Nat. Commun.*, 2023, **14**, 3776.
48 S. Liang, L. Huang, Y. Gao, Q. Wang and B. Liu, *Adv. Sci.*, 2021, **8**, 2102886.
49 D. Karapinar, N. T. Huan, N. Ranjbar Sahraie, J. Li, D. Wakerley, N. Touati, S. Zanna, D. Taverna, L. H. Galvão Tizei, A. Zitolo, F. Jaouen, V. Mougel and M. Fontecave, *Angew. Chem., Int. Ed.*, 2019, **58**, 15098–15103.
50 Q. He, J. H. Lee, D. Liu, Y. Liu, Z. Lin, Z. Xie, S. Hwang, S. Kattel, L. Song and J. G. Chen, *Adv. Funct. Mater.*, 2020, **30**, 2000407.
51 Z. Geng, Y. Cao, W. Chen, X. Kong, Y. Liu, T. Yao and Y. Lin, *Appl. Catal., B*, 2019, **240**, 234–240.
52 J. Li, B. Zhang, B. Dong and L. Feng, *Chem. Commun.*, 2023, **59**, 3523–3535.
53 M. Li, H. Wang, W. Luo, P. C. Sherrell, J. Chen and J. Yang, *Adv. Mater.*, 2020, **32**, 2001848.
54 F. Pan, H. Zhang, K. Liu, D. Cullen, K. More, M. Wang, Z. Feng, G. Wang, G. Wu and Y. Li, *ACS Catal.*, 2018, **8**, 3116–3122.
55 J. Zhang, W. Cai, F. X. Hu, H. Yang and B. Liu, *Chem. Sci.*, 2021, **12**, 6800–6819.
56 S. Wang, L. Wang, D. Wang and Y. Li, *Energy Environ. Sci.*, 2023, **16**, 2759–2803.
57 N. M. Latiff, X. Fu, D. K. Mohamed, A. Veksha, M. Handayani and G. Lisak, *Carbon*, 2020, **168**, 245–253.
58 S. Fu, B. Izelaar, M. Li, Q. An, M. Li, W. de Jong and R. Kortlever, *Nano Energy*, 2025, **133**, 110461.
59 T. Yoshii, K. Chida, H. Nishihara and F. Tani, *Chem. Commun.*, 2022, **58**, 3578–3590.
60 A. B. Sorokin, *Chem. Rev.*, 2013, **113**, 8152–8191.
61 K. Chen, K. Liu, P. An, H. Li, Y. Lin, J. Hu, C. Jia, J. Fu, H. Li, H. Liu, Z. Lin, W. Li, J. Li, Y.-R. Lu, T.-S. Chan, N. Zhang and M. Liu, *Nat. Commun.*, 2020, **11**, 4173.
62 M. Wang, K. Torbensen, D. Salvatore, S. Ren, D. Joulié, F. Dumoulin, D. Mendoza, B. Lassalle-Kaiser, U. Işci, C. P. Berlinguette and M. Robert, *Nat. Commun.*, 2019, **10**, 3602.
63 L. Chen, R. U. R. Sagar, J. Chen, J. Liu, S. Aslam, F. Nosheen, T. Anwar, N. Hussain, X. Hou and T. Liang, *Int. J. Hydrogen Energy*, 2021, **46**, 19338–19346.
64 N. Alzate-Carvajal, L. M. Bolivar-Pineda, V. Meza-Laguna, V. A. Basiuk, E. V. Basiuk and E. A. Baranova, *ChemElectroChem*, 2020, **7**, 428–436.
65 X. Li, X. Wu, Y. Zhao, Y. Lin, J. Zhao, C. Wu, H. Liu, L. Shan, L. Yang, L. Song and J. Jiang, *Adv. Mater.*, 2023, **35**, 2302467.
66 S. Zhou, L.-J. Zhang, L. Zhu, C.-H. Tung and L.-Z. Wu, *Adv. Mater.*, 2023, **35**, 2300923.
67 J. Li, F. Zhang, X. Zhan, H. Guo, H. Zhang, W.-Y. Zan, Z. Sun and X.-M. Zhang, *Chin. J. Catal.*, 2023, **48**, 117–126.
68 X. Yang, J. Cheng, X. Xuan, N. Liu and J. Liu, *ACS Sustainable Chem. Eng.*, 2020, **8**, 10536–10543.
69 D.-D. Ma, S.-G. Han, C. Cao, X. Li, X.-T. Wu and Q.-L. Zhu, *Appl. Catal., B*, 2020, **264**, 118530.
70 S. Liu, H. B. Yang, S.-F. Hung, J. Ding, W. Cai, L. Liu, J. Gao, X. Li, X. Ren, Z. Kuang, Y. Huang, T. Zhang and B. Liu, *Angew. Chem., Int. Ed.*, 2020, **59**, 798–803.
71 K. Chen, M. Cao, Y. Lin, J. Fu, H. Liao, Y. Zhou, H. Li, X. Qiu, J. Hu, X. Zheng, M. Shakouri, Q. Xiao, Y. Hu, J. Li, J. Liu, E. Cortés and M. Liu, *Adv. Funct. Mater.*, 2022, **32**, 2111322.
72 J. He, Y. Han, X. Xu, M. Sun, L. Kang, W. Lin and J. Liu, *J. Mater. Chem. A*, 2025, **13**, 15762–15772.
73 K. Hu, S. Jia, B. Shen, Z. Wang, Z. Dong and H. Lyu, *Chem. Eng. J.*, 2024, **497**, 154686.
74 D.-H. Nam, P. De Luna, A. Rosas-Hernández, A. Thevenon, F. Li, T. Agapie, J. C. Peters, O. Shekhah, M. Eddaoudi and E. H. Sargent, *Nat. Mater.*, 2020, **19**, 266–276.
75 Z. Liang, H.-Y. Wang, H. Zheng, W. Zhang and R. Cao, *Chem. Soc. Rev.*, 2021, **50**, 2540–2581.
76 J.-D. Yi, D.-H. Si, R. Xie, Q. Yin, M.-D. Zhang, Q. Wu, G.-L. Chai, Y.-B. Huang and R. Cao, *Angew. Chem.*, 2021, **133**, 17245–17251.
77 Y. Sano, R. Toyoda, K. Chida, T. Yoshii, H. Nishihara, Y. Nishina, D. Asanoma, S. Takaishi, K. Sugimoto and R. Sakamoto, *ACS Appl. Mater. Interfaces*, 2024, **16**, 42615–42622.
78 A. Trigueros-Sancho, B. Martínez-Sánchez, D. Cazorla-Amorós and E. Morallón, *Carbon*, 2023, **211**, 118100.
79 T. Ogoshi, Y. Sakatsume, K. Onishi, R. Tang, K. Takahashi, H. Nishihara, Y. Nishina, B. D. L. Campéon, T. Kakuta and T.-A. Yamagishi, *Commun. Chem.*, 2021, **4**, 75.
80 J. Coates, Interpretation of Infrared Spectra, a Practical Approach, in *Encyclopedia of Analytical Chemistry*, ed. R. A. Meyers, John Wiley & Sons Ltd, 2006.
81 Z. Li, L. Deng, I. A. Kinloch and R. J. Young, *Prog. Mater. Sci.*, 2023, **135**, 101089.
82 D. B. Schuepfer, F. Badaczewski, J. M. Guerra-Castro, D. M. Hofmann, C. Heiliger, B. Smarsly and P. J. Klar, *Carbon*, 2020, **161**, 359–372.
83 A. Barroso Bogeat, *Crit. Rev. Solid State Mater. Sci.*, 2021, **46**, 1–37.

84 F. Rosenburg, B. Balke, N. Nicoloso, R. Riedel and E. Ionescu, *Molecules*, 2020, **25**, 5919.
85 A. Casotto, G. Drera, D. Perilli, S. Freddi, S. Pagliara, M. Zanotti, L. Schio, A. Verdini, L. Floreano, C. D. Valentin and L. Sangaletti, *Nanoscale*, 2022, **14**, 13166–13177.
86 I. Czekaj, F. Loviat, F. Raimondi, J. Wambach, S. Biollaz and A. Wokaun, *Appl. Catal., A*, 2007, **329**, 68–78.
87 S. Gong, S. Yang, W. Wang, R. Lu, H. Wang, X. Han, G. Wang, J. Xie, D. Rao, C. Wu, J. Liu, S. Shao and X. Lv, *Small*, 2023, **19**, 2207808.
88 Y. Wang, Z. Jiang, X. Zhang, Z. Niu, Q. Zhou, X. Wang, H. Li, Z. Lin, H. Zheng and Y. Liang, *ACS Appl. Mater. Interfaces*, 2020, **12**, 33795–33802.
89 Y. J. Sa, H. Jung, D. Shin, H. Y. Jeong, S. Ringe, H. Kim, Y. J. Hwang and S. H. Joo, *ACS Catal.*, 2020, **10**, 10920–10931.
90 C. Yan, H. Li, Y. Ye, H. Wu, F. Cai, R. Si, J. Xiao, S. Miao, S. Xie, F. Yang, Y. Li, G. Wang and X. Bao, *Energy Environ. Sci.*, 2018, **11**, 1204–1210.
91 M. Shirai, M. Arai and K. Murakami, *J. Synchrotron Radiat.*, 2001, **8**, 584–586.
92 H. Nishihara, T. Hirota, K. Matsuura, M. Ohwada, N. Hoshino, T. Akutagawa, T. Higuchi, H. Jinnai, Y. Koseki, H. Kasai, Y. Matsuo, J. Maruyama, Y. Hayasaka, H. Konaka, Y. Yamada, S. Yamaguchi, K. Kamiya, T. Kamimura, H. Nobukuni and F. Tani, *Nat. Commun.*, 2017, **8**, 109.
93 K. Chida, T. Yoshii, K. Takahashi, M. Yamamoto, K. Kanamaru, M. Ohwada, V. Deerattrakul, J. Maruyama, K. Kamiya, Y. Hayasaka, M. Inoue, F. Tani and H. Nishihara, *Chem. Commun.*, 2021, **57**, 6007–6010.
94 Q. Chang, Y. Liu, J.-H. Lee, D. Ologunagba, S. Hwang, Z. Xie, S. Kattel, J. H. Lee and J. G. Chen, *J. Am. Chem. Soc.*, 2022, **144**, 16131–16138.
95 M. Zhu, R. Ye, K. Jin, N. Lazouski and K. Manthiram, *ACS Energy Lett.*, 2018, **3**, 1381–1386.
96 Z. Zhang, J. Xiao, X.-J. Chen, S. Yu, L. Yu, R. Si, Y. Wang, S. Wang, X. Meng, Y. Wang, Z.-Q. Tian and D. Deng, *Angew. Chem., Int. Ed.*, 2018, **57**, 16339–16342.
97 Q. Wang, K. Liu, K. Hu, C. Cai, H. Li, H. Li, M. Herran, Y.-R. Lu, T.-S. Chan, C. Ma, J. Fu, S. Zhang, Y. Liang, E. Cortés and M. Liu, *Nat. Commun.*, 2022, **13**, 6082.